Flash Graphene from Plastic Waste—Supporting Information

Wala A. Algozeeb,[1] Paul E. Savas,[1] Duy Xuan Luong,[1] Weiyin Chen,[1] Carter Kittrell,[1] Mahesh Bhat,[2] Rouzbeh Shahsavari,[2] and James M. Tour[,1,3,4]*

[1]Department of Chemistry, Rice University, 6100 Main Street, Houston, Texas 77005, USA

[2]C-Crete Technologies, Stafford, TX, USA

[3]Department of Materials Science and NanoEngineering, Rice University, 6100 Main Street, Houston, Texas 77005, USA

[4]Smalley-Curl Institute, NanoCarbon Center and Welch Institute for Advanced Materials, Rice University, 6100 Main Street, Houston, Texas 77005, USA

**Email: tour@rice.edu*

DC circuit description

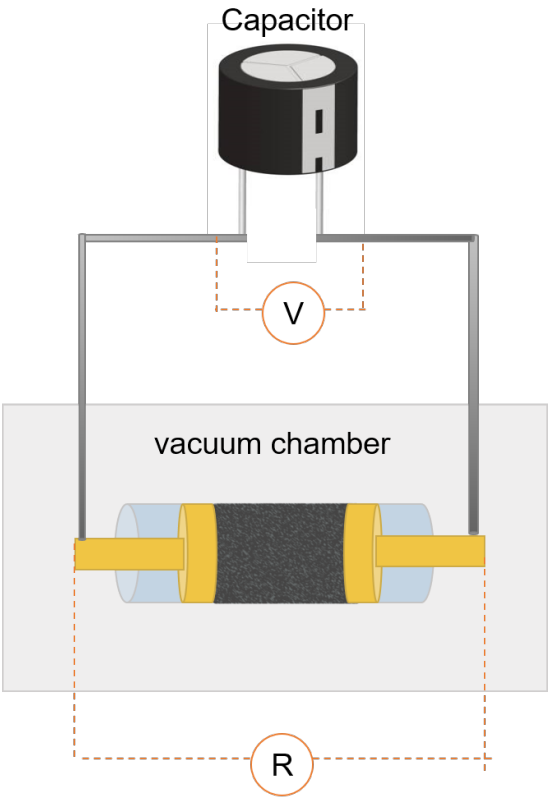

Figure S1. Simplified scheme of the DC-FJH setup. Detailed description of the circuit was reported in previous work.[1]

Alternating current flash Joule heating (AC-FJH) Equipment Description

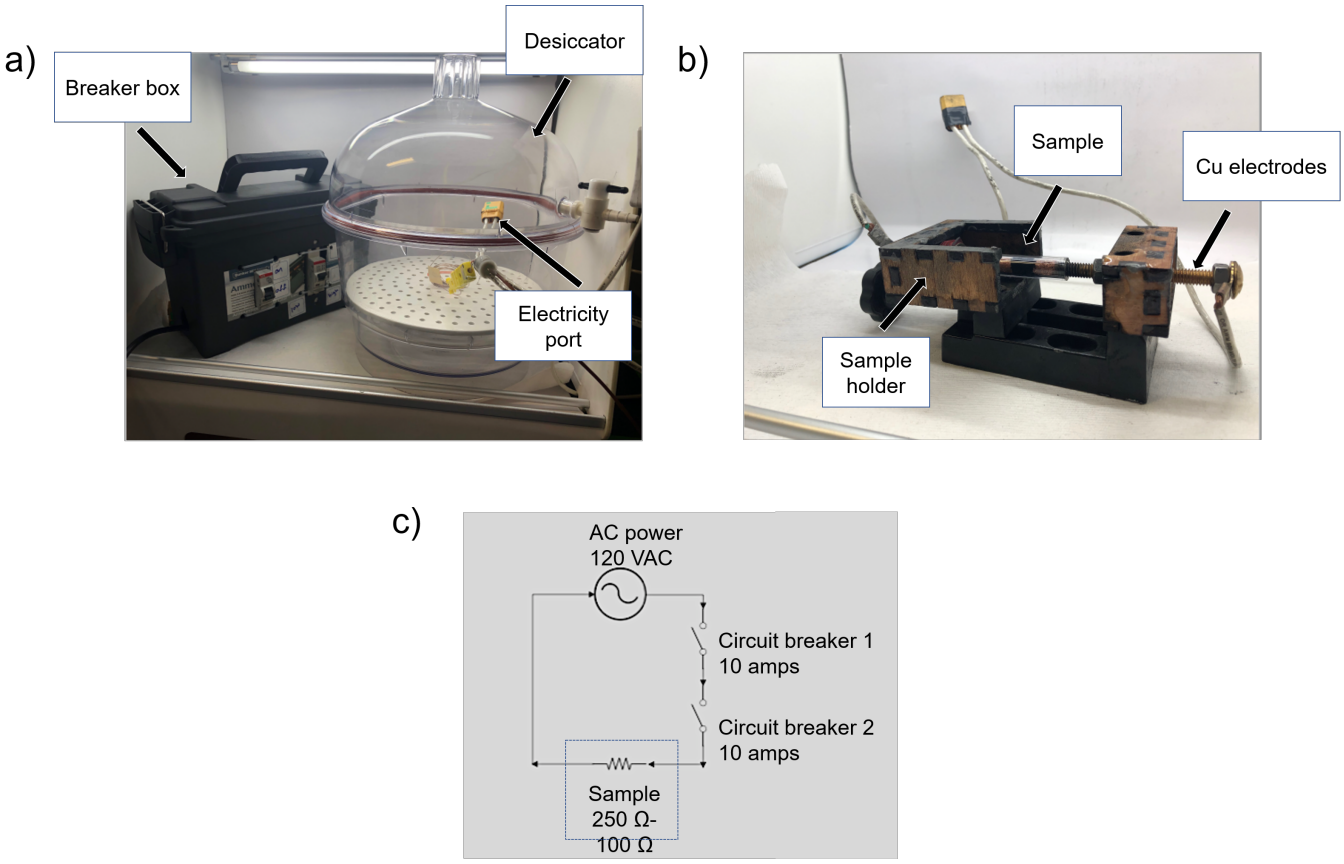

Figure S2. Pictures of the AC-FJH equipment for pretreating PW samples. a) The sample holder is placed in a plastic desiccator for protection of the operator. The 10 amp breaker box and electrical ports into the desiccator are indicated by labels. b) A close-up view of the sample holder, sample, and copper electrodes. c) Circuit diagram of the AC-FJH equipment.

The AC setup is comprised of a plastic desiccator for safety, a sample holder and two 10 amp breaker box.

CAUTION: Flash Joule heating (FJH) involves high current, which may cause electrical shock or even electrocution. This list is not intended to be comprehensive, but demonstrative of the protocols needed to minimize risk.

- Samples subjected to FJH must be enclosed in a container or fume hood for safety. There is chance of tube breakage during the FJH.
- Vacuum is required to remove volatiles generated upon FJH. Volatiles can ignite and catch fire if not properly vented.
- All wires must be enclosed and well insulated.
- All wires must be rated for high current.
- It is recommended that users use double rubber gloves when working with the FJH system.
- One hand rule. Use only one hand when working on the system, with the other hand not touching any grounded surface.
- Use an IR protective googles to protect your eyes from the bright flash. Glasses designed for welding are generally suitable because they effectively block infrared as well as ultraviolet.
- Detailed safety measures for dealing with the DC-FJH system was included in previous work.[1]

Raman Spectral Analysis

Whenever the D-band is present, there is a weaker D' (disorder) band at ~1620 cm^{-1} that usually appears as a shoulder on the high frequency side of the G-band causing a slight asymmetry. The D'-band is a weak longitudinal optical phonon band that occurs with the D-band and will always be present when the D-band is large.[2] The D'-band does not depend on the type of edge. Unlike

the much stronger D-band, zigzag edges will contribute to the D'-band.[3] Since the intensity of the D'-band is much weaker that of the D-band and very close to the larger G-peak, the zigzag edge contribution is often too small to observe it. Because AC-FG usually has higher D-band intensity, some of the AC-FG Raman spectra show a slight band that is outside the green Lorentzian fitted curve due to the presence of the D' bulge in the G band.

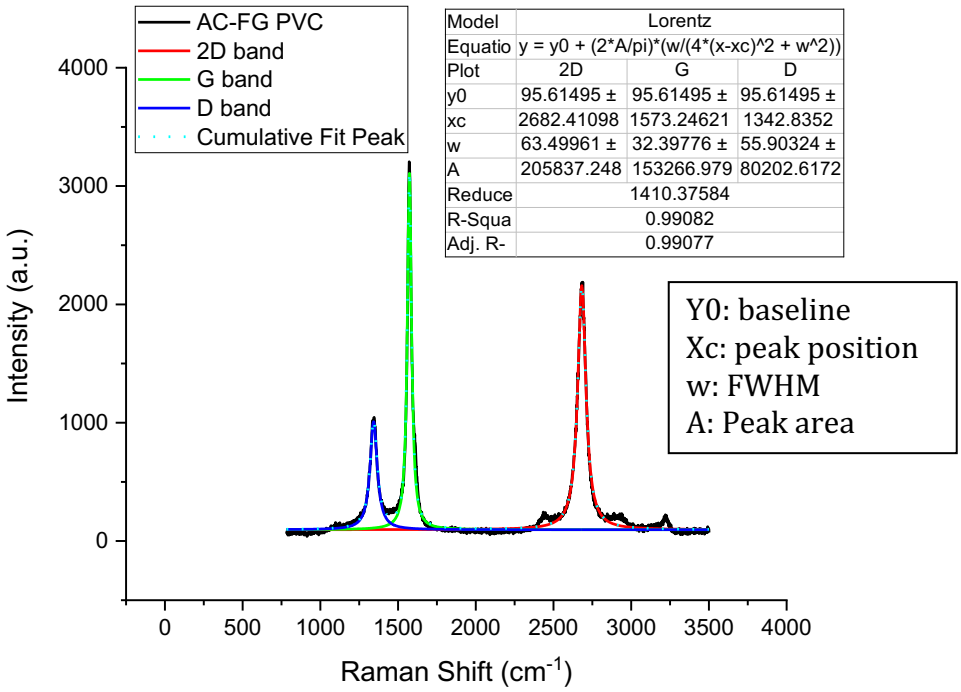

Figure S3. Raman fitting of the AC-FG from PET.

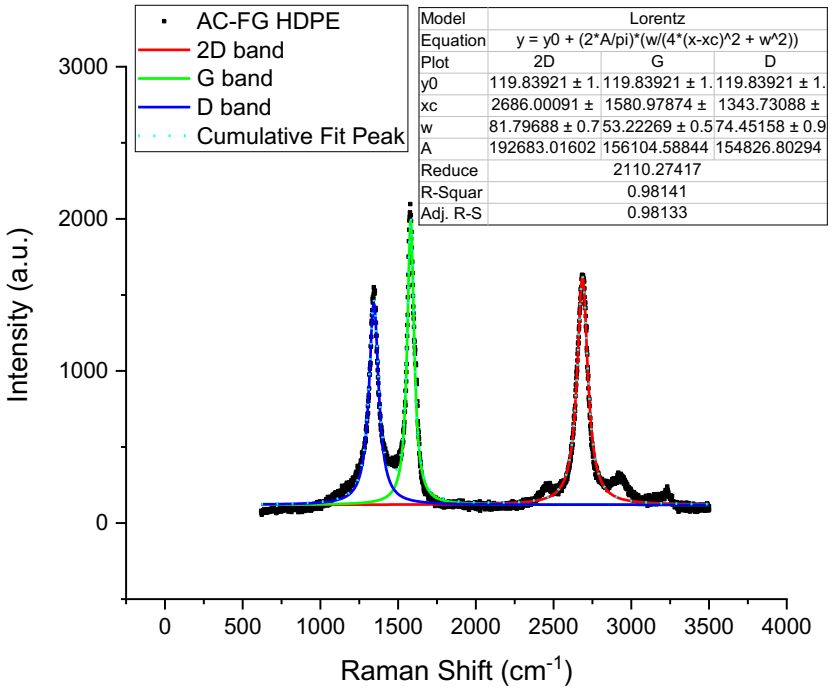

Model	Lorentz		
Equation	y = y0 + (2*A/pi)*(w/(4*(x-xc)^2 + w^2))		
Plot	2D	G	D
y0	119.83921 ± 1.	119.83921 ± 1.	119.83921 ± 1.
xc	2686.00091 ±	1580.97874 ±	1343.73088 ±
w	81.79688 ± 0.7	53.22269 ± 0.5	74.45158 ± 0.9
A	192683.01602	156104.58844	154826.80294
Reduce	2110.27417		
R-Squar	0.98141		
Adj. R-S	0.98133		

Figure S4. Raman fitting of the AC-FG from HDPE.

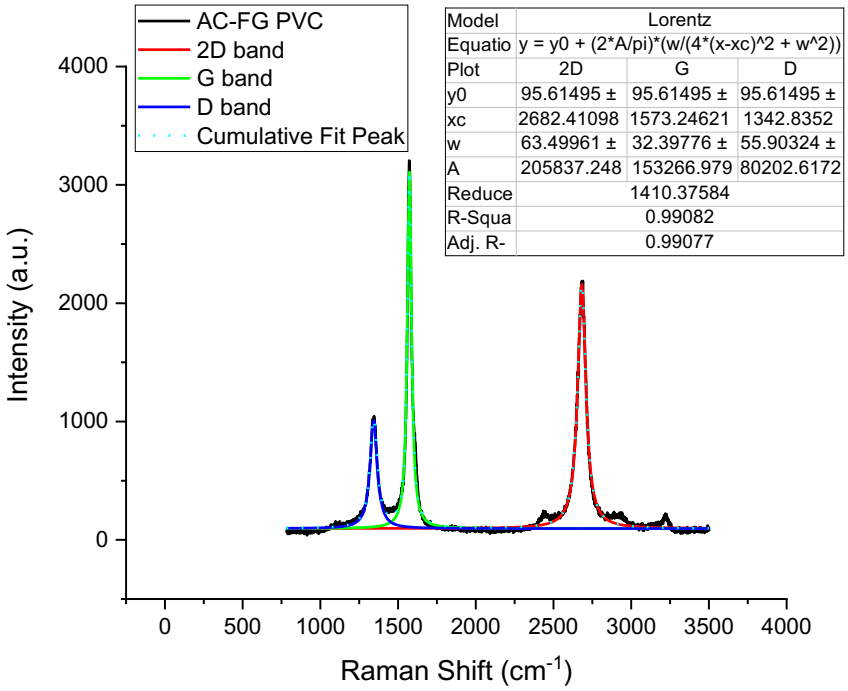

Model	Lorentz		
Equatio	y = y0 + (2*A/pi)*(w/(4*(x-xc)^2 + w^2))		
Plot	2D	G	D
y0	95.61495 ±	95.61495 ±	95.61495 ±
xc	2682.41098	1573.24621	1342.8352
w	63.49961 ±	32.39776 ±	55.90324 ±
A	205837.248	153266.979	80202.6172
Reduce	1410.37584		
R-Squa	0.99082		
Adj. R-	0.99077		

Figure S5. Raman fitting of the AC-FG from PVC.

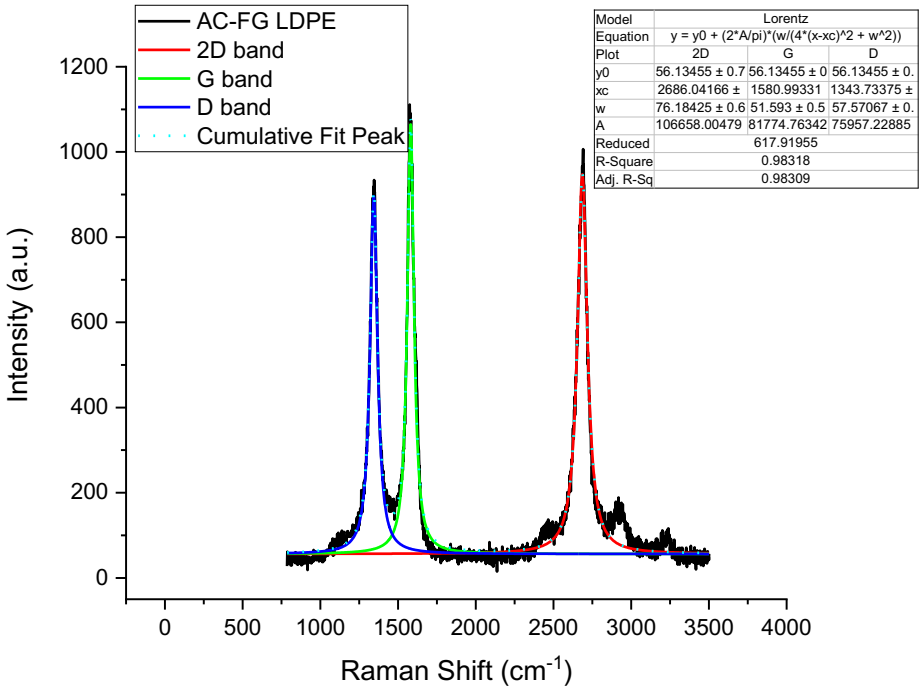

Model	Lorentz		
Equation	y = y0 + (2*A/pi)*(w/(4*(x-xc)^2 + w^2))		
Plot	2D	G	D
y0	56.13455 ± 0.7	56.13455 ± 0	56.13455 ± 0.
xc	2686.04166 ±	1580.99331	1343.73375 ±
w	76.18425 ± 0.6	51.593 ± 0.5	57.57067 ± 0.
A	106658.00479	81774.76342	75957.22885
Reduced	617.91955		
R-Square	0.98318		
Adj. R-Sq	0.98309		

Figure S6. Raman fitting of the AC-FG from LDPE.

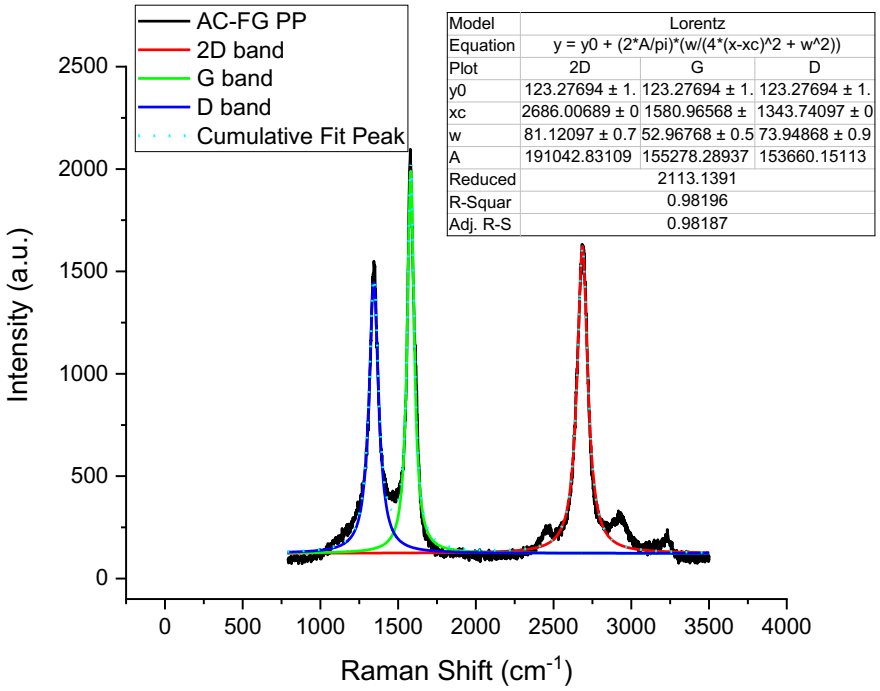

Model	Lorentz		
Equation	y = y0 + (2*A/pi)*(w/(4*(x-xc)^2 + w^2))		
Plot	2D	G	D
y0	123.27694 ± 1.	123.27694 ± 1.	123.27694 ± 1.
xc	2686.00689 ± 0	1580.96568 ±	1343.74097 ± 0
w	81.12097 ± 0.7	52.96768 ± 0.5	73.94868 ± 0.9
A	191042.83109	155278.28937	153660.15113
Reduced	2113.1391		
R-Squar	0.98196		
Adj. R-S	0.98187		

Figure S7. Raman fitting of the AC-FG from PP.

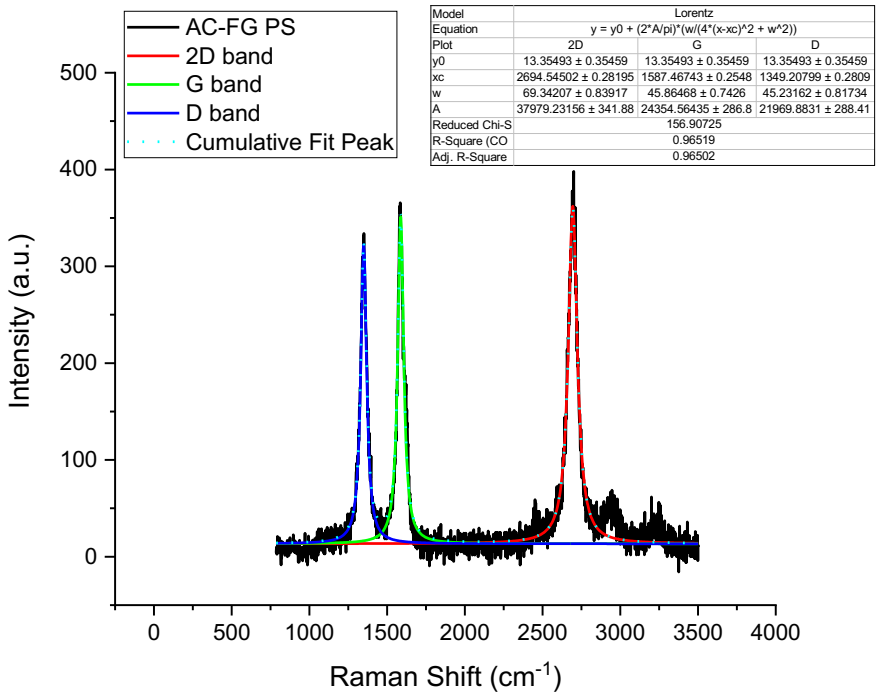

Model	Lorentz		
Equation	y = y0 + (2*A/pi)*(w/(4*(x-xc)^2 + w^2))		
Plot	2D	G	D
y0	13.35493 ± 0.35459	13.35493 ± 0.35459	13.35493 ± 0.35459
xc	2694.54502 ± 0.28195	1587.46743 ± 0.2548	1349.20799 ± 0.2809
w	69.34207 ± 0.83917	45.86468 ± 0.7426	45.23162 ± 0.81734
A	37979.23156 ± 341.88	24354.56435 ± 286.8	21969.8831 ± 288.41
Reduced Chi-S	156.90725		
R-Square (CO	0.96519		
Adj. R-Square	0.96502		

Figure S8. Raman fitting of the AC-FG from PS.

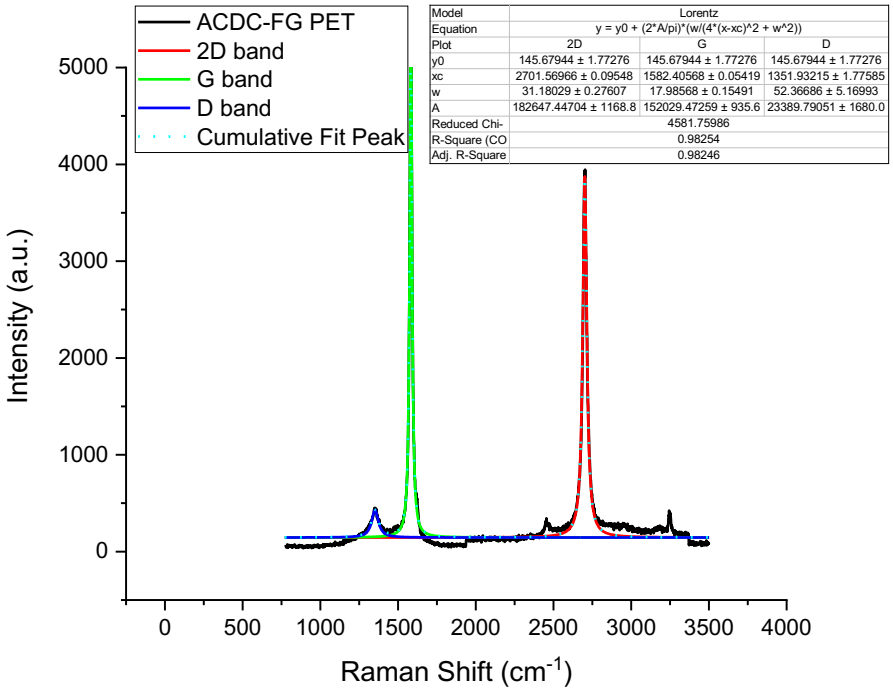

Model	Lorentz		
Equation	y = y0 + (2*A/pi)*(w/(4*(x-xc)^2 + w^2))		
Plot	2D	G	D
y0	145.67944 ± 1.77276	145.67944 ± 1.77276	145.67944 ± 1.77276
xc	2701.56966 ± 0.09548	1582.40568 ± 0.05419	1351.93215 ± 1.77585
w	31.18029 ± 0.27607	17.98568 ± 0.15491	52.36686 ± 5.16993
A	182647.44704 ± 1168.8	152029.47259 ± 935.6	23389.79051 ± 1680.0
Reduced Chi-	4581.75986		
R-Square (CO	0.98254		
Adj. R-Square	0.98246		

Figure S9. Raman fitting of the ACDC-FG from PET.

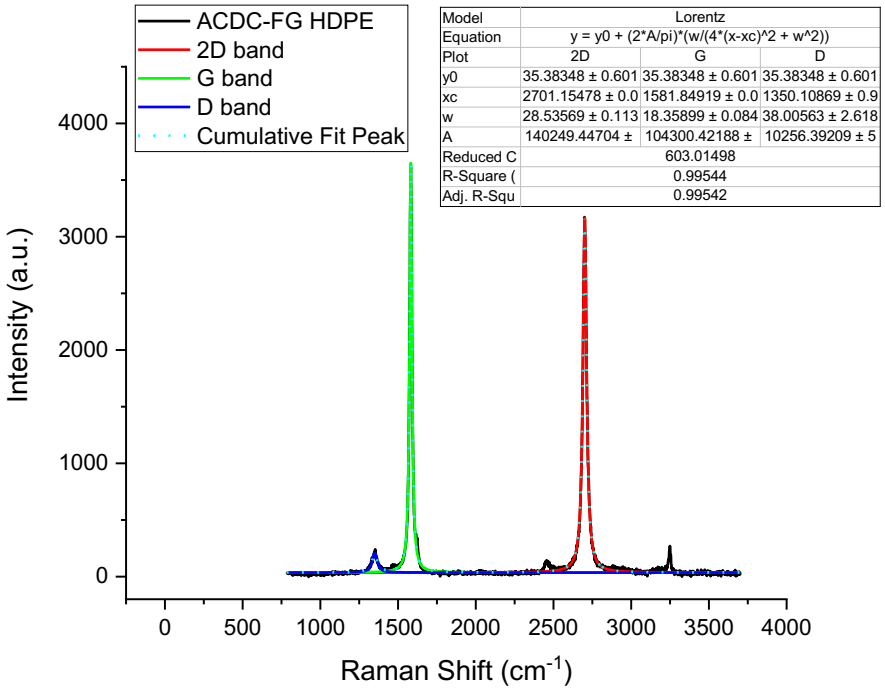

Figure S10. Raman fitting of the ACDC-FG from HDPE.

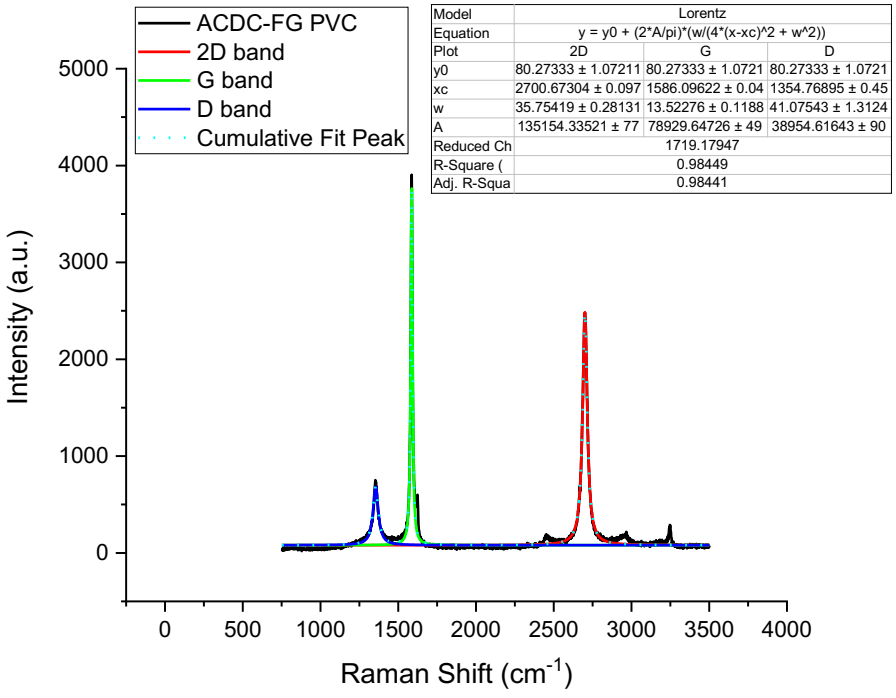

Figure S11. Raman fitting of the ACDC-FG from PVC.

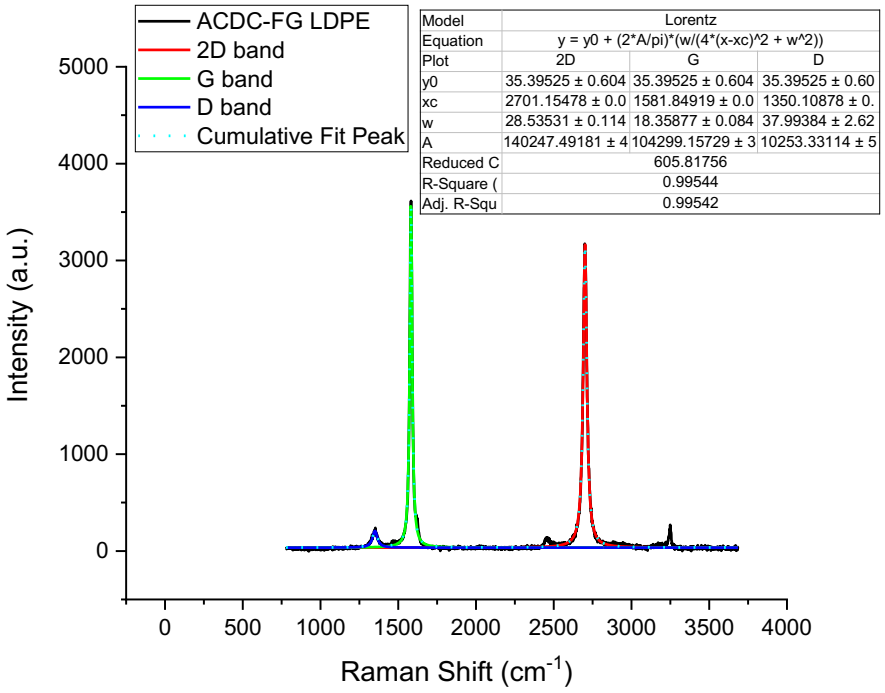

Model	Lorentz		
Equation	y = y0 + (2*A/pi)*(w/(4*(x-xc)^2 + w^2))		
Plot	2D	G	D
y0	35.39525 ± 0.604	35.39525 ± 0.604	35.39525 ± 0.60
xc	2701.15478 ± 0.0	1581.84919 ± 0.0	1350.10878 ± 0.
w	28.53531 ± 0.114	18.35877 ± 0.084	37.99384 ± 2.62
A	140247.49181 ± 4	104299.15729 ± 3	10253.33114 ± 5
Reduced C	605.81756		
R-Square (	0.99544		
Adj. R-Squ	0.99542		

Figure S12. Raman fitting of the ACDC-FG from LDPE.

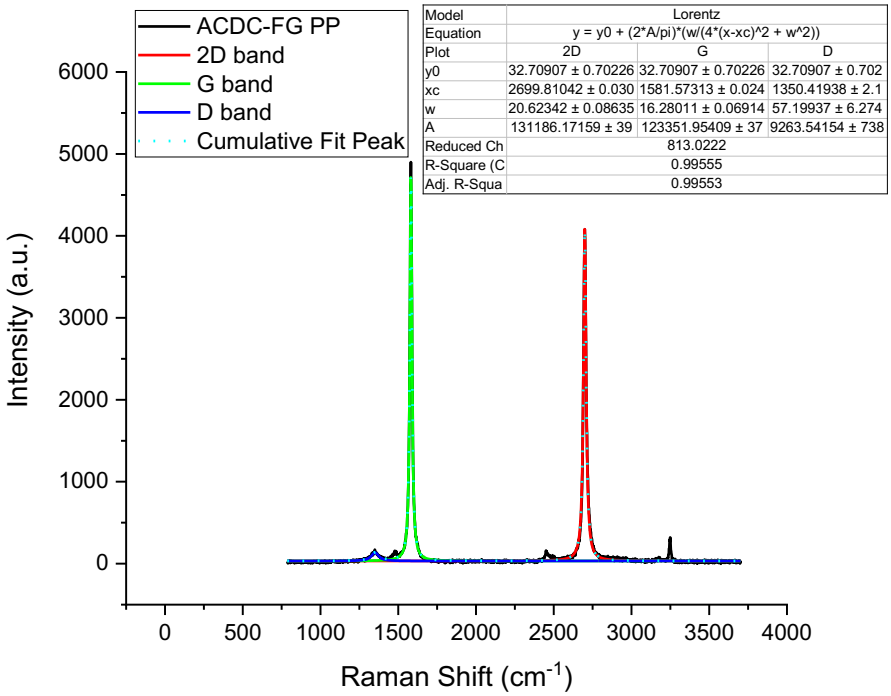

Model	Lorentz		
Equation	y = y0 + (2*A/pi)*(w/(4*(x-xc)^2 + w^2))		
Plot	2D	G	D
y0	32.70907 ± 0.70226	32.70907 ± 0.70226	32.70907 ± 0.702
xc	2699.81042 ± 0.030	1581.57313 ± 0.024	1350.41938 ± 2.1
w	20.62342 ± 0.08635	16.28011 ± 0.06914	57.19937 ± 6.274
A	131186.17159 ± 39	123351.95409 ± 37	9263.54154 ± 738
Reduced Ch	813.0222		
R-Square (C	0.99555		
Adj. R-Squa	0.99553		

Figure S13. Raman fitting of the ACDC-FG from PP.

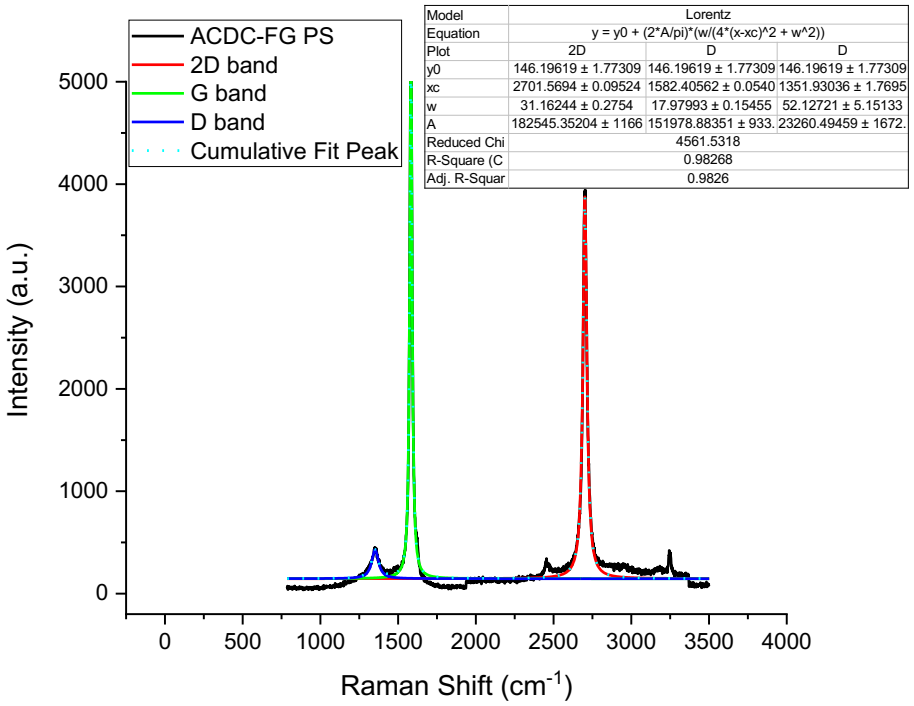

Model	Lorentz		
Equation	y = y0 + (2*A/pi)*(w/(4*(x-xc)^2 + w^2))		
Plot	2D	D	D
y0	146.19619 ± 1.77309	146.19619 ± 1.77309	146.19619 ± 1.77309
xc	2701.5694 ± 0.09524	1582.40562 ± 0.0540	1351.93036 ± 1.7695
w	31.16244 ± 0.2754	17.97993 ± 0.15455	52.12721 ± 5.15133
A	182545.35204 ± 1166	151978.88351 ± 933.	23260.49459 ± 1672.
Reduced Chi	4561.5318		
R-Square (C	0.98268		
Adj. R-Squar	0.9826		

Figure S14. Raman fitting of ACDC-FG from PS.

Key Indicators of the Formation of High Quality tFG from Raman Spectra

1. I_D/I_G band ratio is a good measure of defect density.

Cancado (*et al.*) demonstrated that the I_D/I_G ratio is a reliable measure of disorder, which is linear in the reciprocal of the nanocrystallite size as determined by XRD.[4] Schmuker (*et al.*) showed that the I_D/I_G ratio is a much more sensitive indicator and grows rapidly with increased number of defects, whereas the 2D peak was minimally affected until the defect density is large.[5]

2. A good Lorentzian fit

For SLG and TSG, there is a fully conical Dirac cone at the K-point, which gives rise to the clean Lorentzian band shape. AB stacking and disorder introduce additional states, which lead to additional transitions and degradation of the Lorentzian band shape.[6,7]

3. The 2D peak for multilayer TS graphene is 2700 cm^{-1} with 532 nm excitation

Garlow (*et al*.) and Niilisk (*et al*.) both show the 2D peak at the same location (after correcting for dispersion), and they have verified by electron microscopy the high quality of the CVD graphene, as shown in Table S1 of the Supplementary Information of our own paper.[1,6,7]

4. The 2D/G peak height ratio is an indicator of the number of turbostratic layers as long as it also fits the criteria of 2 and 3, a good Lorentzian fit that is not too broad and at the correct frequency for the peak. The 2D/G ratio is a less sensitive indicator of quality than the D/G ratio.[8]

AC *vs* DC pretreatment

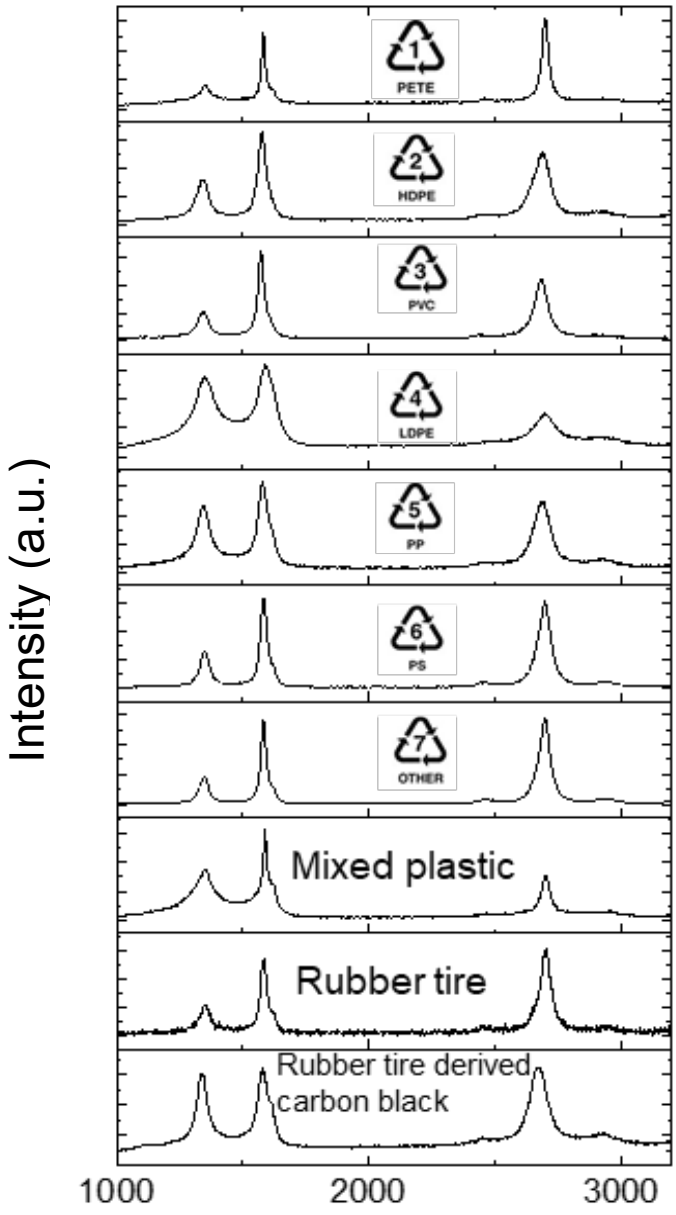

Figure S15. Characteristic Raman spectra of PW FG produced *via* direct DC-FJH without the AC pretreatment as reported from reference 1.

Figure S16 shows TGA of FG obtained *via* DC flashing of HDPE at different voltages compared to FG obtained via AC-FG. For each of the DC-flashed sample, HDPE was flashed 5 times at the specified voltage with a discharge time of 500 ms. A DC-FJH pretreatment of plastic was found to insufficient for full carbonization of plastic waste compared to AC-FG, which shows no residual plastic in TGA.

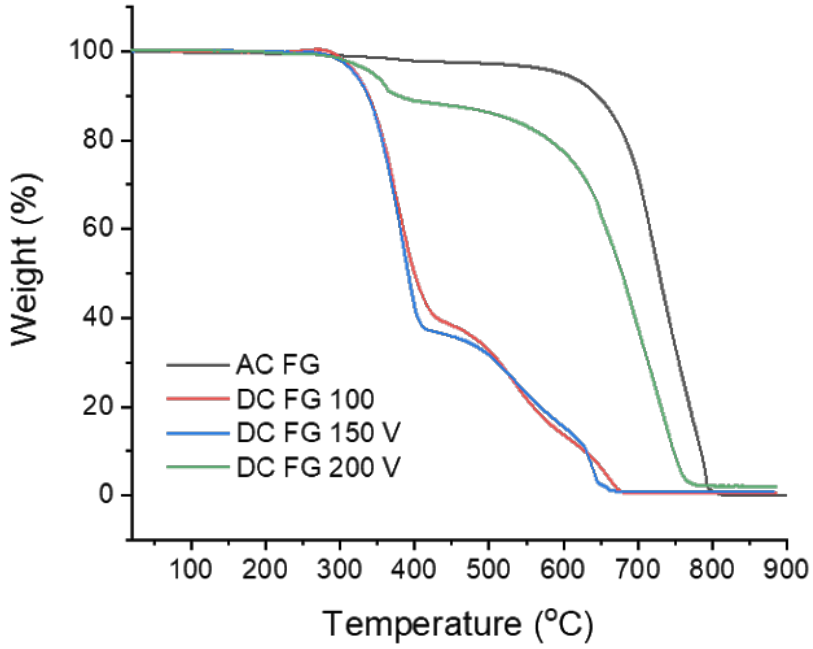

Figure S16. TGA (air, 15 °C/min) of HDPE-derived FG prepared at different voltages.

Tarping IR and UV light during FJH

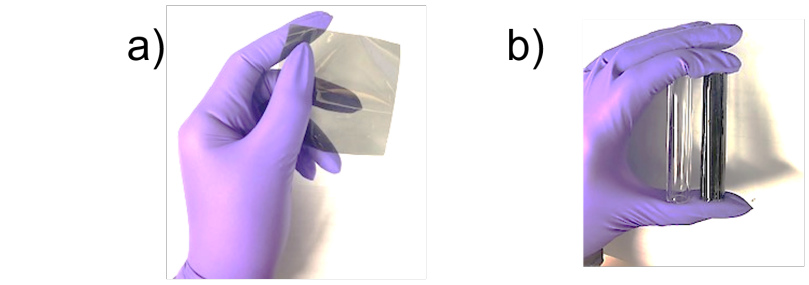

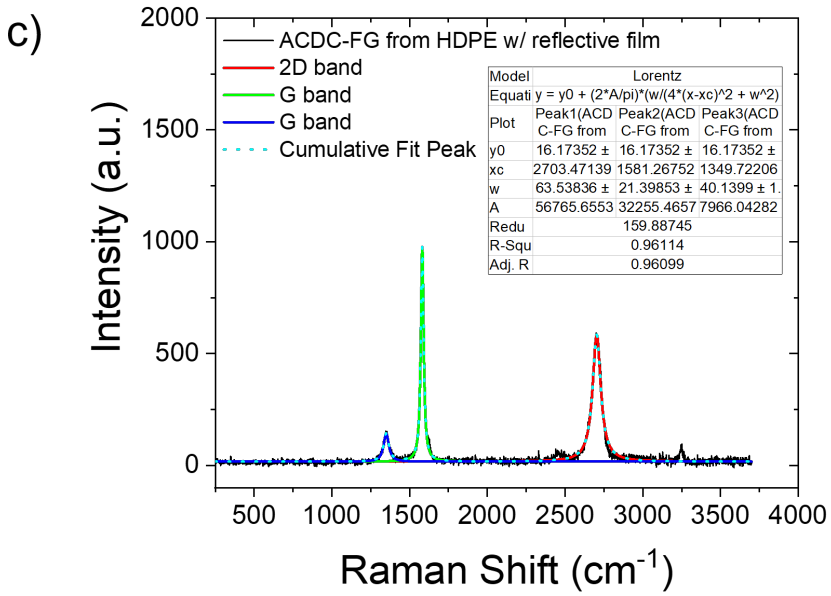

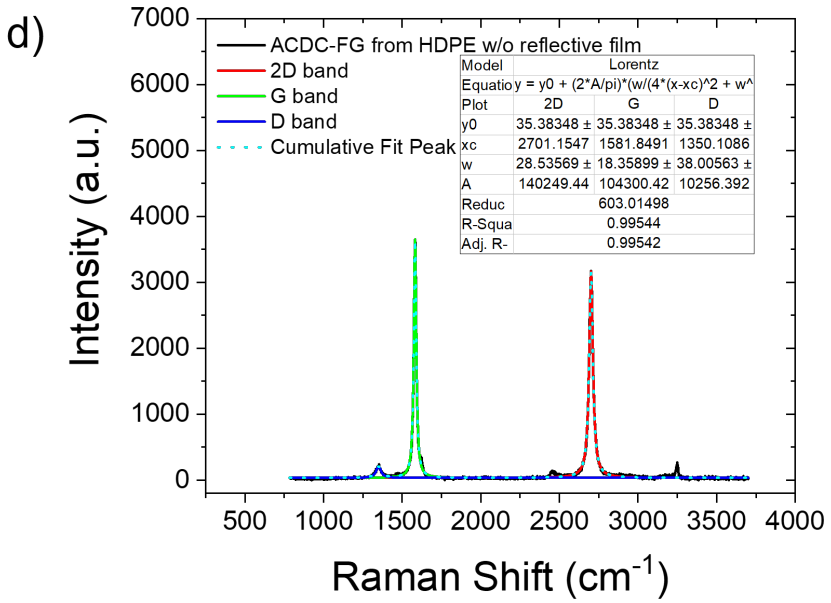

Figure S17. a) Picture of the nanoceramic IR/UV reflective film. b) Picture of the flashing quartz tube with and without the film. Raman fitting of ACDC-FG from HDPE. c) Raman fitting of ACDC-FG from HDPE with reflective film showing poor Lorentzian fitting ($R^2 = 0.96$). d) Raman fitting of ACDC-FG from HDPE without reflective film showing good Lorentzian fitting ($R^2 = 0.99$)

IR spectrometer components

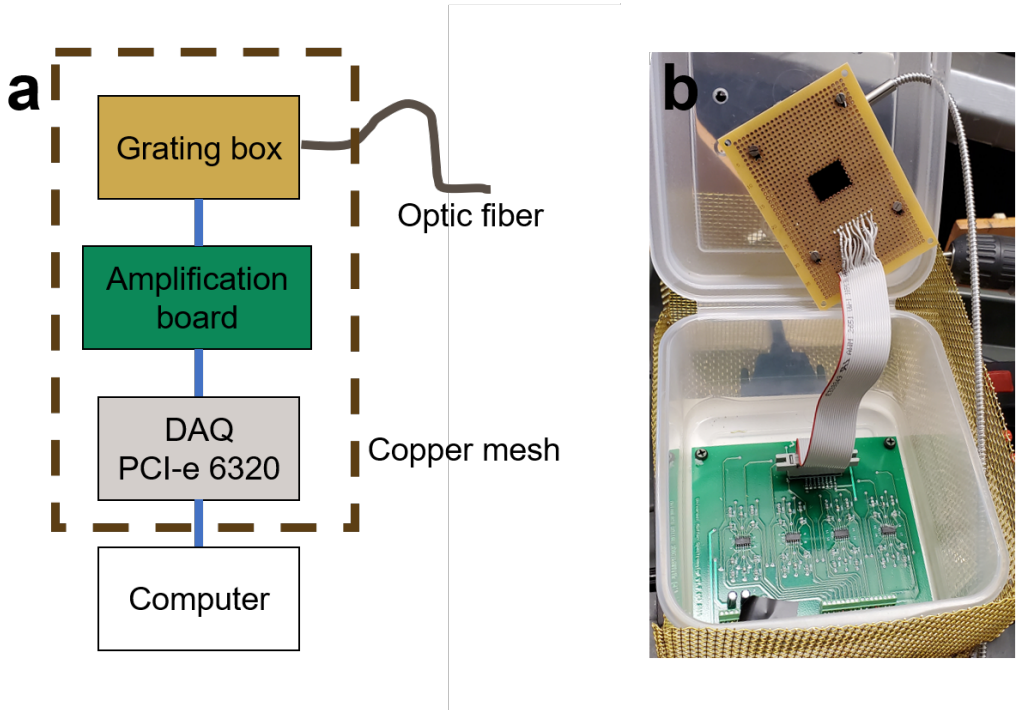

Figure S18. Components of the IR spectrometer built in-house for temperature determination. a) Schematic of the spectrometer. The grating box scatters light from 600-1000 nm and collects the spectrum with a 16-channel photodiode array. The signal from the photodiode arrays is amplified by the amplification board from 16 op-amps. The signal is then collected by the DAQ PCI-e 6320.

The computer processes the data to the spectrum and fits it with black body radiation curve. The system is enclosed inside a copper mesh to reduce noise. b) Photo of the spectrometer.

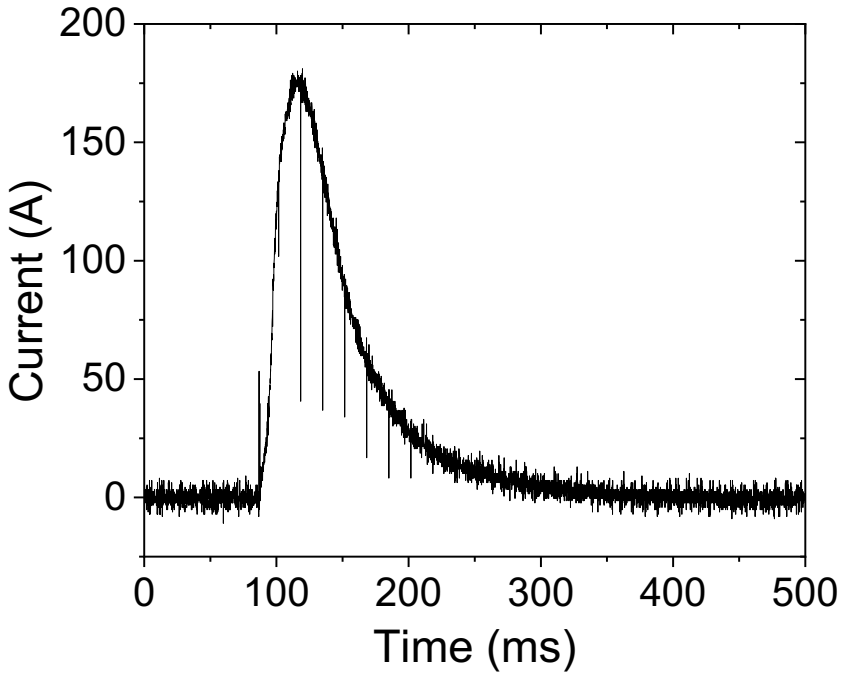

Figure S19. Recording of the current passing through the AC-FG during DC-FJH process

TGA of FG

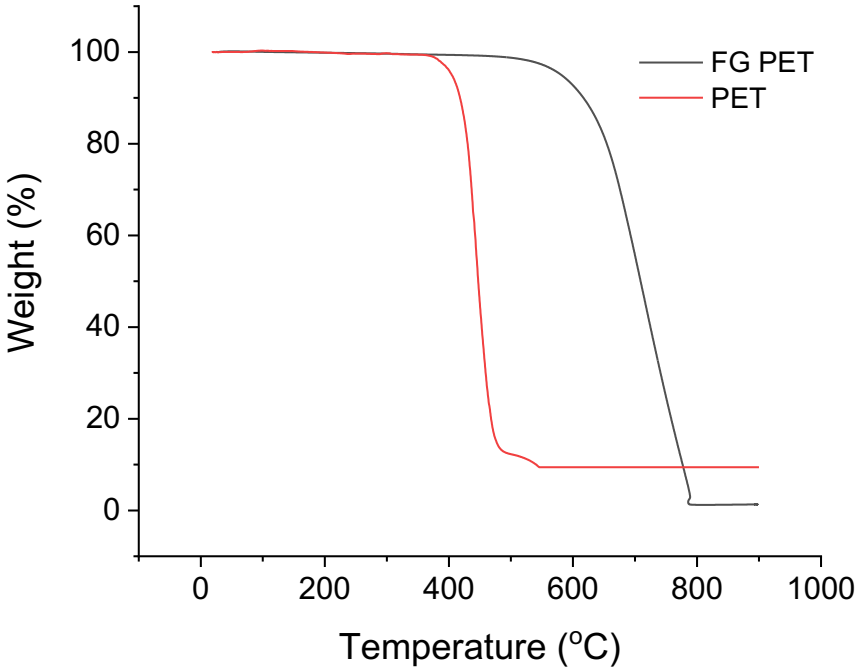

Figure S20. TGA (air, 15 °C/min) of PET before and after AC-FJH. The thermogram for FG derived from PET goes to 0 wt% at 790 °C showing that the ~10 wt% nanoclays residue in PET has been volatilized in the flashing process.

XRD of tFG from Different Plastics

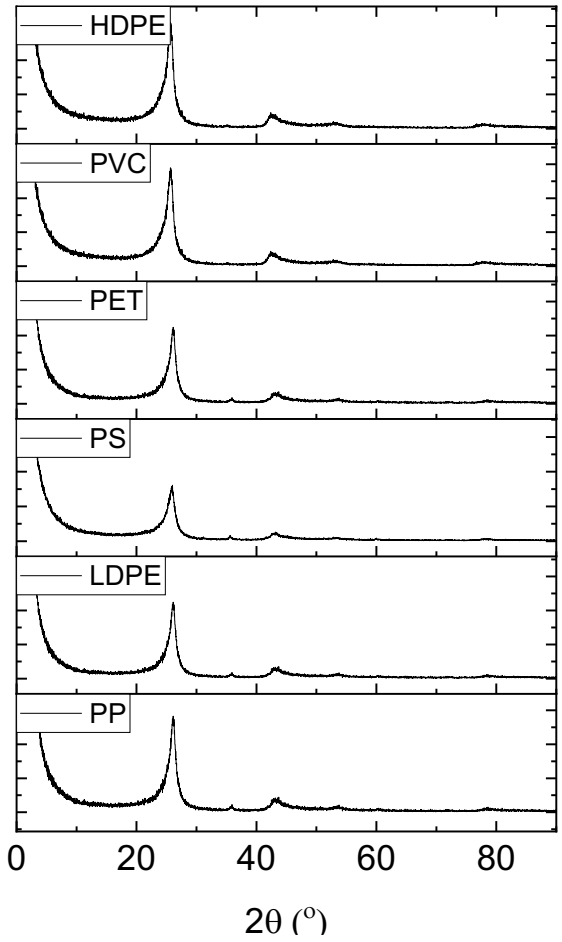

Figure S21. XRD of ACDC-tFG obtained for different plastics.

XPS of FG from different plastics

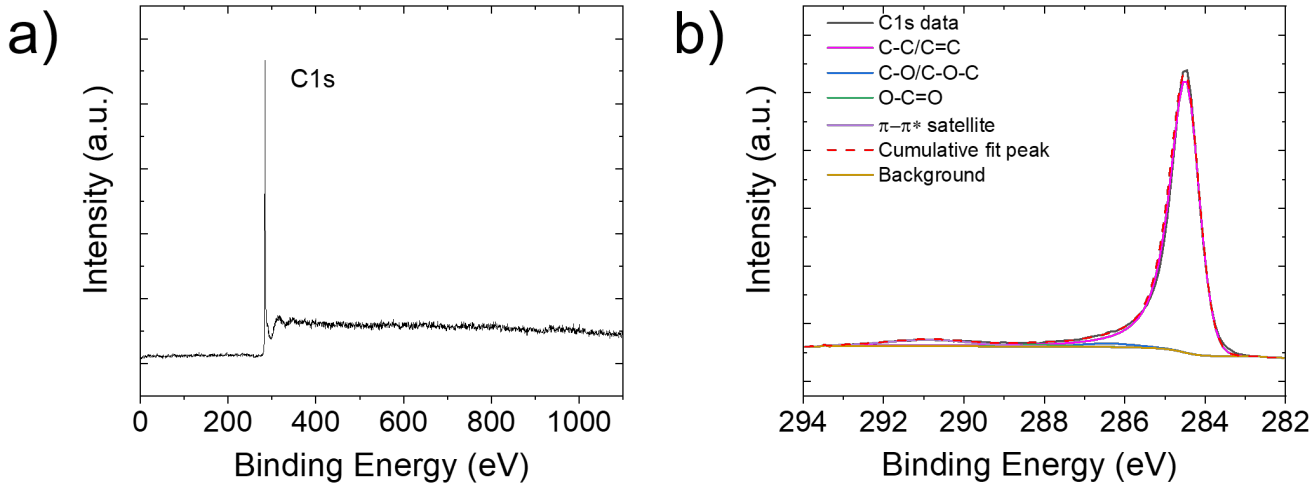

Figure S22. a) Survey scan and b) high resolution C1s XPS FG from PVC showing no deteted chlorine in the FG matrix.

Layer count and interlayer spacing using TEM images

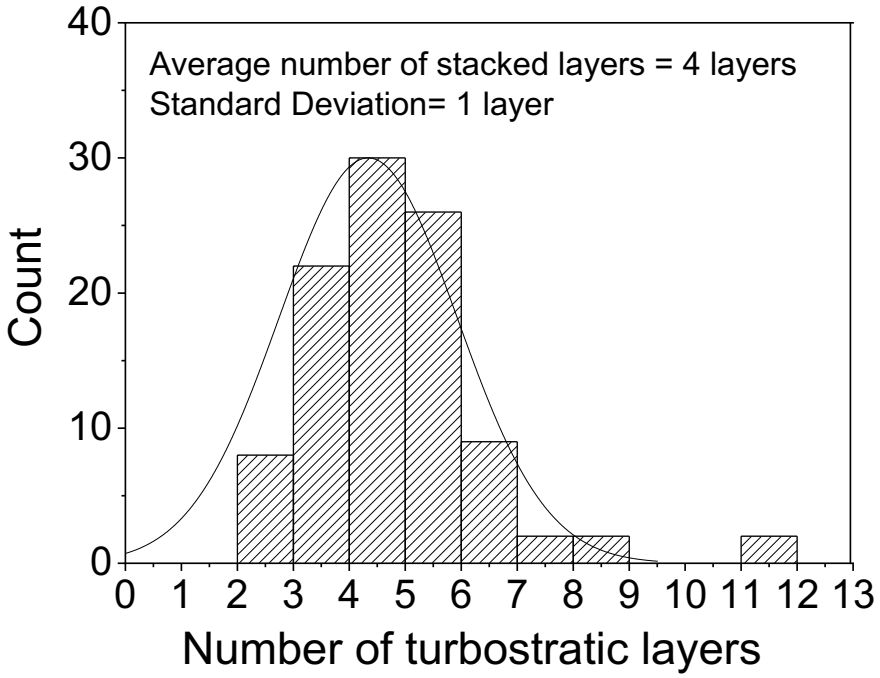

Figure S23. Turbostratic layers count of AC-FG (n = 100).

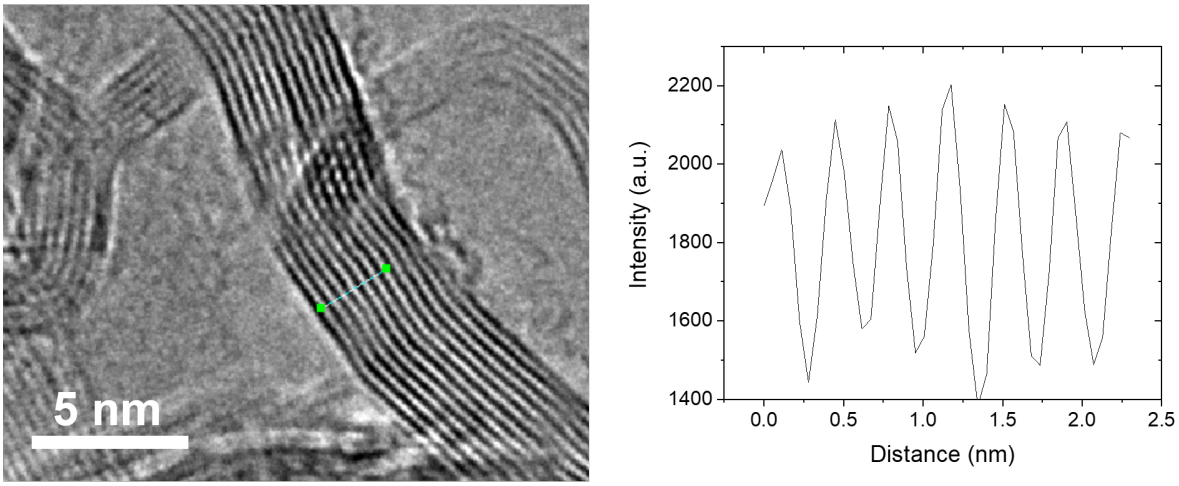

Figure S24. Interlayer distance of AC-FG.

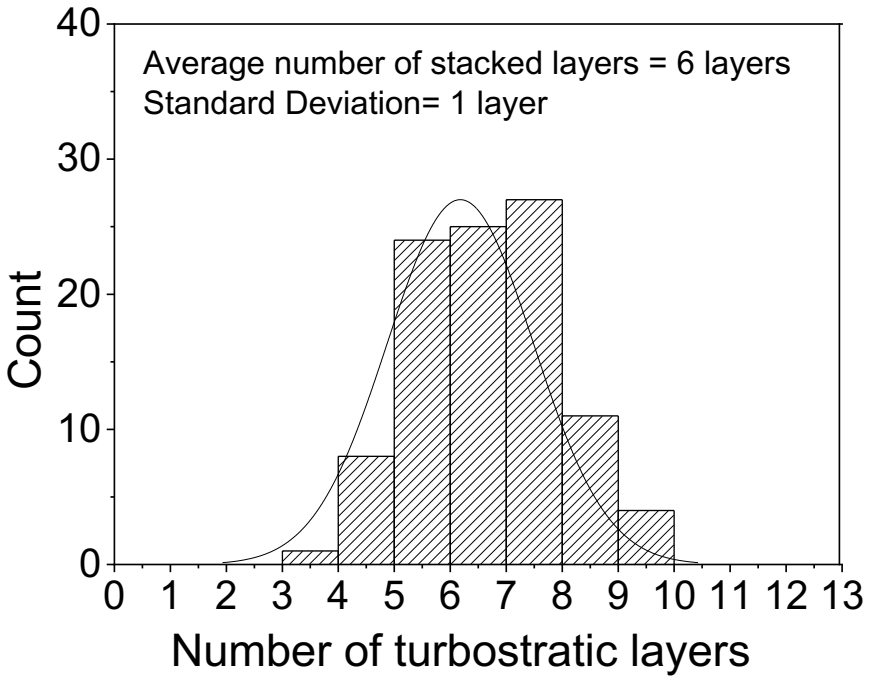

Figure S25. Turbostratic layers count of ACDC-tFG (n = 100).

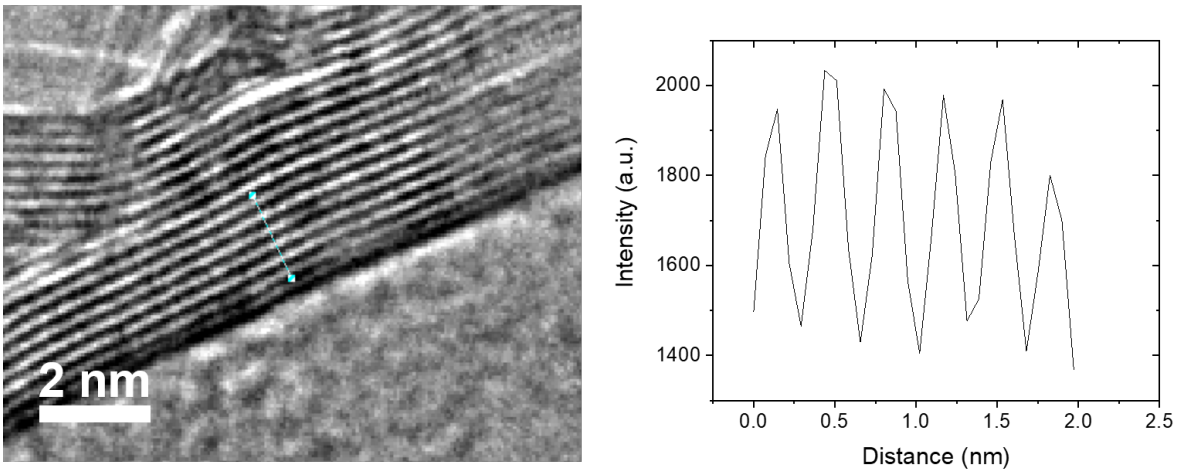

Figure S26. Interlayer distance of ACDC-FG.

Cost of converting graphene to plastic

To calculate the power needed to produce FG from PW, the resistance across the PW sample was recorded at different times. Equation 1 was used to calculate the power.

$$P = V^2 / R \quad (1)$$

Where P is power

V is the voltage, which is 120 V throughout the experiment.

R is the resistance

The calculated power was then integrated overtime to obtain the consumed kWh.

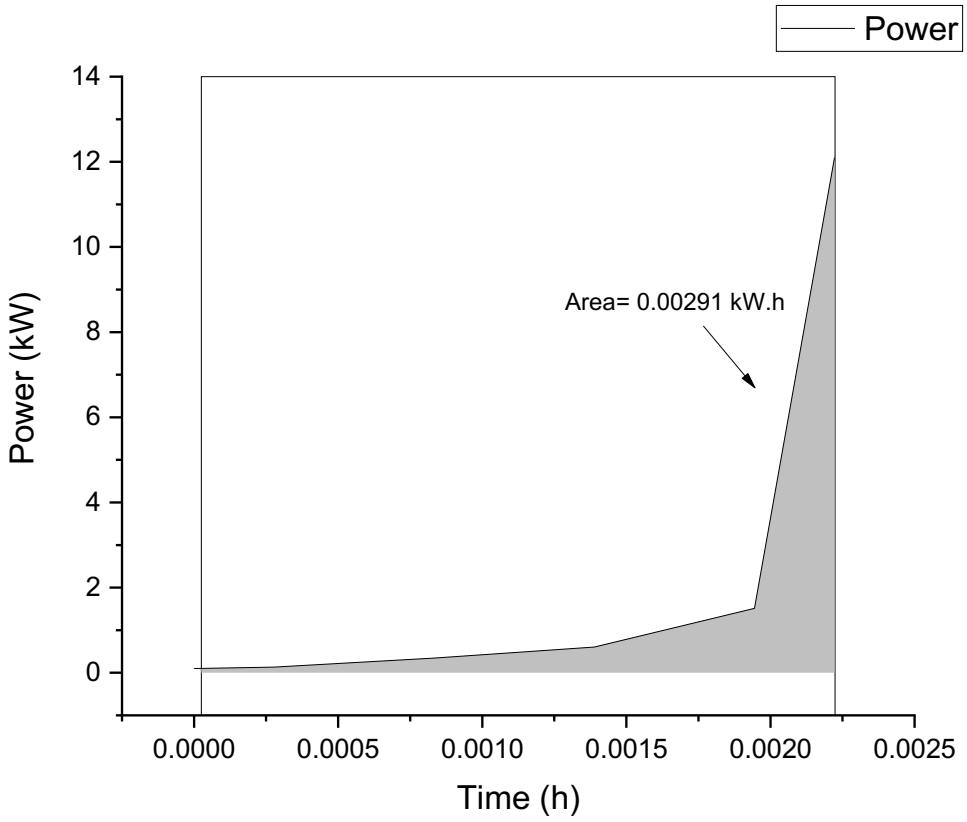

.

Figure S27. Power require to carbonize 0.5 g of mixed plastic in the AC system

The total power consumed to convert plastic waste to FG was calculated to be 5.8 Wh/g (0.00582 kW/g). So, for 1 ton of plastic, 5261725 Wh will be consumed (5361.72 kWh/ton). Given that the

industrial price of electric energy in Texas, USA is $0.02/kWh, the total cost for carbonizing 1 ton of plastic is ~ $107.

kJ conversion: 5.8 W×h/g is ~ 20880 J/g (20.9 kJ/g).

Price of DC flashing of graphene from the AC system.

- The flashing voltage was set to 110 V for 100 mg.
- The discharge time was found to be 0.1 s. Initial resistance is 1 Ω and final resistance is 0.8 Ω.
- The total power consumed is 3.6 Wh/g, which is around 13 kJ/g.
- The total cost is $65/ton to upgrade the quality of graphene

Price of the AC and DC process combined 107 (AC) + 16.25 (DC) = $124/ton of plastic

Table S1. Average price of virgin and recycled plastic in Q4 of 2019

Plastic Type	PET ($/ton)	HDPE ($/ton)	LDPE ($/ton)	PP ($/ton)	PS ($/ton)	PVC ($/ton)
Virgin Plastic	1405	1080	1025	1036	1477	780-845
Recycled Plastic	1513	1647	1173	1130	2417	777

Collecting and analyzing the waxes from FJH plastic waste

To analyze the waxes generated during the flashing process, the waxes are collected in a glass wool trap. Upon FJH, the evolved gases and waxes are withdrawn by vacuum, and higher molecular weight waxes are trapped in the glass wool. Dichloromethane was used to extract the waxes for analysis. Schematic of the setup is shown in Figure S28a. Figure 28b shows a picture of the glass wool with wax deposited on it prior to IR analysis.

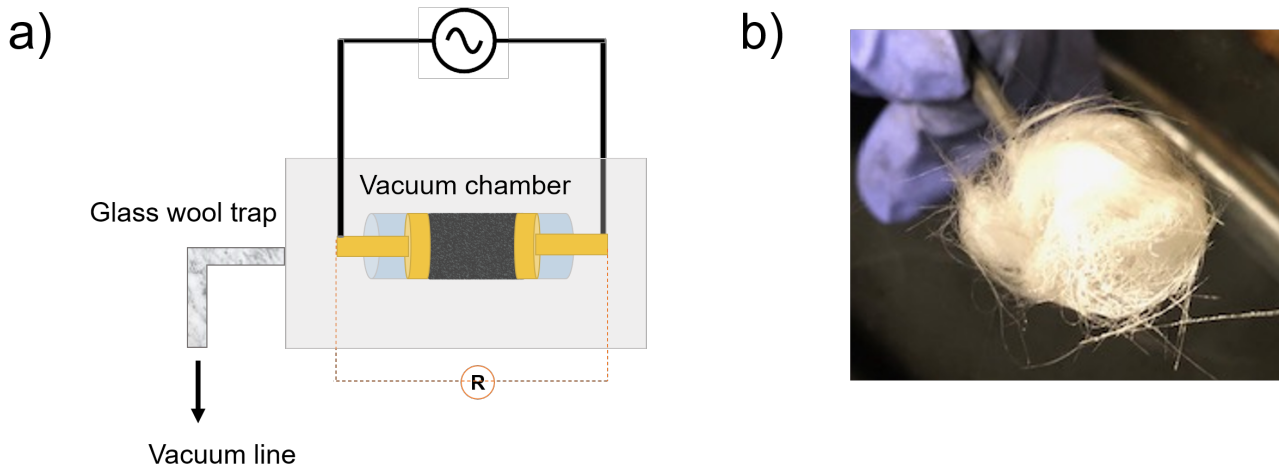

Figure S28. a) Schematic of the glass wool trap to collect the waxes. b) Picture of the glass wool with waxes deposited on it after FJH plastics.

Analysis of the evolved gases

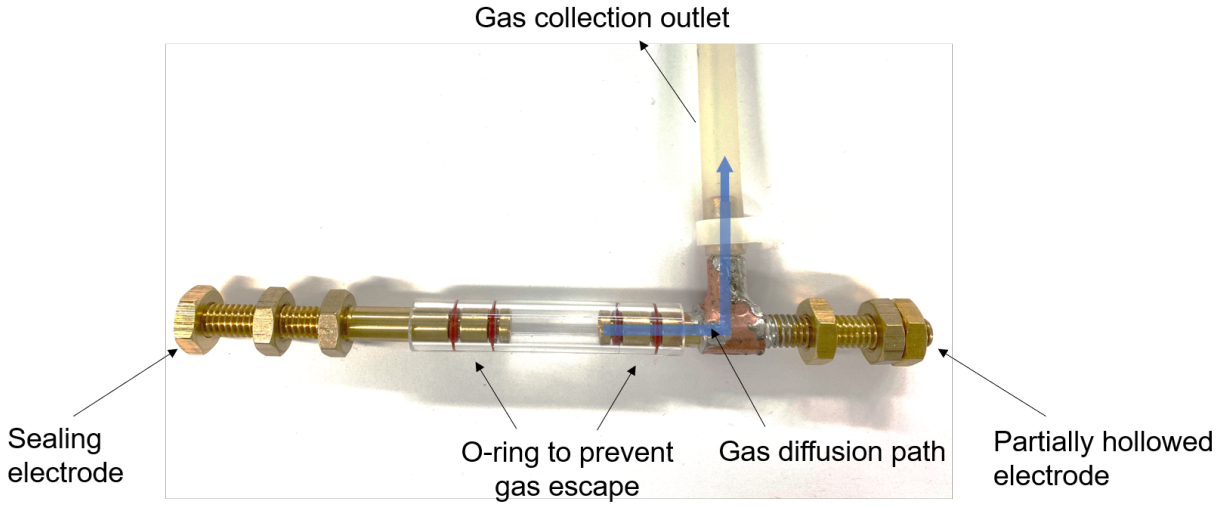

Figure S29. Picture of the electrodes designed for gas capture upon FJH. The amount of hydrogen is estimated by recording the pressure change when cooling from room temperature to -196 °C. The estimate of the amount of hydrogen is reliable because it should be the only significant component at -196 °C, since methane has about 10 Torr vapor pressure at -196 °C. The hydrogen was then pumped off to allow the other gases to condense at the bottom. A small amount of methane would also be removed during the brief pump out. When the trap is warmed from -196 °C to -78 °C (dry ice), the second fraction, which constitutes methane + 2 and 3 carbon moieties evaporates. The relatively slow rise in pressure upon removal from the liquid nitrogen suggests that methane is a minor component, but further analysis is needed using GC-MS to determine these proportions.

References

1. Luong, D. X.; Bets, K. V.; Algozeeb, W. A.; Stanford, M. G.; Kittrell, C.; Chen, W.; Salvatierra, R. V.; Ren, M.; McHugh, E. A.; Advincula, P. A.; Wang, Z.; Bhatt, M.; Guo, H.;

Mancevski, V.; Shahsavari, R.; Yakobson, B. I.; Tour, J. M. Gram-Scale Bottom-up Flash Graphene Synthesis. *Nature* **2020**, *577*, 647-651.

2. Martins Ferreira, E. H.; Moutinho, M. V. O.; Stavale, F.; Lucchese, M. M.; Capaz, R. B.; Achete, C. A.; Jorio, A. Evolution of the Raman Spectra From Single-, Few-, and Many-Layer Graphene with Increasing Disorder. *Phys. Rev. B* **2010**, *82*, 125429.

3. Pimenta, M. A.; Dresselhaus, G.; Dresselhaus, M. S.; Cançado, L. G.; Jorio, A.; Saito, R. Studying Disorder in Graphite-Based Systems by Raman Spectroscopy. *Phys. Chem. Chem. Phys.* **2007**, *9*, 1276-1290.

4. Cançado, L. G.; Takai, K.; Enoki, T.; Endo, M.; Kim, Y. A.; Mizusaki, H.; Jorio, A.; Coelho, L. N.; Magalhães-Paniago, R.; Pimenta, M. A. General Equation for the Determination of the Crystallite Size L_a of Nanographite by Raman Spectroscopy. *Appl. Phys. Lett.* **2006**, *88*, 163106.

5. Schmucker, S. W.; Cress, C. D.; Culbertson, J. C.; Beeman, J. W.; Dubon, O. D.; Robinson, J. T. Raman Signature of Defected Twisted Bilayer Graphene. *Carbon* **2015**, *93*, 250-257.

6. Niilisk, A.; Kozlova, J.; Alles, H.; Aarik, J.; Sammelselg, V., Raman Characterization of Stacking in Multi-Layer Graphene Grown on Ni. *Carbon* **2016**, *98*, 658-665.

7. Garlow, J. A.; Barrett, L. K.; Wu, L.; Kisslinger, K.; Zhu, Y.; Pulecio, J. F. Large-Area Growth of Turbostratic Graphene on Ni(111) *via* Physical Vapor Deposition. *Sci. Rep.* **2016**, *6*, 19804.

8. Hwang, J. S.; Lin, Y. H.; Hwang, J. Y.; Chang, R.; Chattopadhyay, S.; Chen, C. J.; Chen, P.; Chiang, H. P.; Tsai, T. R.; Chen, L. C.; Chen, K. H. Imaging Layer Number and Stacking Order Through Formulating Raman Fingerprints Obtained From Hexagonal Single Crystals of Few Layer Graphene. *Nanotechnology* **2012**, *24*, 015702.